

ORNL/TM-2007/105

TIME-DEPENDENT DEFORMATION MODELLING FOR A CHOPPED-GLASS-FIBER COMPOSITE FOR AUTOMOTIVE DURABILITY DESIGN CRITERIA

Weiju Ren*

Metals and Ceramics Division
Oak Ridge National Laboratory
Oak Ridge, TN 3783 1-6155

ABSTRACT

Time-dependent deformation behavior of a polymeric composite with chopped-glass-fiber reinforcement was investigated for automotive applications. The material under stress was exposed to representative automobile service environments. Results show that environment has substantial effects on time-dependent deformation behavior of the material. The data were analyzed and experimentally-based models developed for the time-dependent deformation behavior as a basis for automotive structural durability design criteria.

Keywords: polymeric composite; automobile; time-dependent deformation; environmental effects; Durability.

1. Introduction

In searching for structural materials for light-weight and fuel-efficient automobiles, fiber-reinforced polymeric composites are considered as promising candidates for applications such as

* Present affiliation: Air Force Research Laboratory, Room 23, Building 655, 2230 Tenth Street, Wright-Patterson Air Force Base, Ohio 45433-7817, U. S. A., Fax: 937-656-4840, Email: Weiju.Ren@afit.af.mil
Oak Ridge National Laboratory, managed by UT-Battelle, LLC, for the U. S. Department of Energy under contract DE-AC05-00OR22725.

floor pans, body side **frames**, cross-members and **front** structural members [1-4]. In addition to stress-rupture as a durability concern [5], polymeric composites under stress also undergo significant time-dependent deformation induced by creep. For the design life of 15 year long-term automotive structural applications with dimensional stability requirements, this time-dependent deformation, especially its response to various automotive service environments, must be fully understood as a durability issue for design purposes. This paper is dedicated to the **time-dependent** deformation behavior of a glass-fiber-reinforced polymeric composite that is considered as a candidate material for automotive structural applications by the Automotive Composites Consortium. The present investigation is a parallel study to that on the stress-rupture behavior of the same candidate material [5], and is a part of the U. S. Department of Energy Advanced Automotive Materials project “Durability of Lightweight Composite Structures for Automotive Applications”. The primary goal of this investigation is to develop **experimentally-based**, time-dependent deformation-driven design guidelines to assure the 15 year long-term integrity of polymeric composite automotive structures. The material was tested in representative automotive service environments. Results were analyzed and time-dependent deformation models were developed for design use.

2. Material

The **material** was a polymeric composite with a urethane-based matrix reinforced by 28.9 vol.% of 50 mm chopped E-glass fibers. The matrix was identified as Baydur 420 IMR produced Bayer Corporation. The IMR denotes “internal mold release”. The chopped fiber preform was made by the P4 process recently developed by Owens-Corning in **Battice**, Belgium. The matrix consisted of polyols and polymeric isocyanates with an amine coreactant to produce a **cross-linked** urea-urethane basic structure. The urea component contributed to the heat resistance of

the final composite structure. Detailed information about the material can be found in reference [6].

3. Text Matrix

Automotive materials are subjected to various service environments including cold and hot weather, engine heat, dry air in deserts, damp air in coastlands, exposure to fluids in a rain or car wash, spill of coolant, windshield washer fluid, brake fluid, motor oil, and battery acid, plus motor vibration and low frequency load cycling on a rough road. The test matrix was designed to simulate the representative service environments, which were selected as “necessary for testing” by narrowing down from the more extensive list of automotive environments studied in a previous investigation on a reference material [4, 7]. The representative environments included lab ambient air with an annual average 50% relative humidity (**Air/50%RH**), distilled water immersion, and windshield washer fluid immersion. The test stress ranged from compressive 125 **MPa** to tensile 155 **MPa**, while the test temperature ranged from -40 to 120°C, but not in all environments. A total of 131 creep tests were conducted, but only those that fell within the stress-strain linear range, which will be defined later, were incorporated into the model development.

4. Experimental Procedures and Data Reduction

For tests under tension, **dogbone** shape specimens having the nominal size of 203.2 x 25.4 x 3.18 mm with a 20.3 mm wide gage section were utilized. For tests under compression, short tablet specimens were employed with a nominal size of 3 1.75 x 25.4 x 3.18 mm. The shortened length was designed to prevent buckling, and both ends of the specimen were machined parallel to each other to ensure a uniform stress distribution when compressed.

The tests were conducted in lever-arm creep machines. Reliable and inexpensive grips were developed to hold the specimens during creep to generate time-dependent deformation data [5]. Because the mechanical response of the material is sensitive to loading rate, all tests were loaded at a constant nominal strain rate of 0.04/min. (6.7 x 10%). The deformation was measured using type CEA-13-SOOUW-350 strain gages (Measurements Group, Inc.) with a 12.7 mm gage length. The gages were bonded to the specimen with M-bond 200 adhesive and protected by a wax coating when tested in fluids at 50°C and below. When testing at 120°C, M-bond GA-61 was employed. The deformation signals from the strain gages were collected electronically using the LabView data acquisition system on desktop computers. More detailed experimental procedures can be found in the parallel study on stress-rupture [53].

As in the investigation on stress-rupture behavior [5], an effort was made to minimize data scatter, mostly resulting from local variation of fiber content, by multiplying the strain with a normalization factor. The normalization factor shown in eqn (1) is the reciprocal of that used in the stress-rupture study [5]:

$$\text{normalized strain} = \text{measured strain} \times (E_{\text{specimen}}/E_{\text{average}}) \quad (1)$$

where

E_{specimen} = Young's modulus of the specimen in air at 23°C,

E_{average} = average Young's modulus of the material in air at 23°C.

An average Young's modulus value of 11.7 **GPa** was used. The normalized strain values were employed for data analysis and model development. In addition to the normalization, two hypotheses were used in the model development.

1. The models were formulated to represent the average time-dependent deformation behavior of the material in view of the severe difference in creep performance and the limited creep data.
2. The models were developed to describe the time-dependent deformation as if no stress rupture had occurred.

The second hypothesis was employed to cover all the specimens with data scatter in various stress-rupture lives. Therefore the deformation models should be applied with the stress-rupture criteria developed in a parallel study [5].

It should also be noted that since the required automotive design life is 15 years with 3,000 to 5,000 operating hours and the tests were conducted for less than 1 year, the uncertainty in design margins must be addressed.

5. Results and Discussion

5.1. Baseline time-dependent deformation

5.1.1. Creep deformation data in air with 50% relative humidity at room temperature under tension

Tensile creep testing at room temperature (23°C) in the lab ambient air with an annual average of 50% relative humidity (**Air/50%RH**) is referred to as the baseline test condition, with which results from the other testing environments were compared. A total of 33 specimens fabricated from plaques B2, B3, and B9 were tested in the baseline condition, and of these 33 tests, 21 were tested within the so-called stress-strain linear range and employed for time-dependent deformation

modeling. The linear range refers to where the creep deformation is a linear function of applied stress.

Part of the baseline experimental data is presented in Fig. 1, from which two features can be observed. First, the deformation was obviously time-dependent. Secondly, at a given time, the deformation increased with the increase in applied stress. If data scatter is ignored, the deformation appears to increase proportionally to the applied stress in the range at 125 MPa and below. Therefore, all the curves within this range in Fig. 1 should collapse into a single curve in terms of unit stress.

5.1.2. Linearity, Data Reduction and Model Development

For linear deformation to occur, two conditions should be satisfied:

1. Strain is proportional to the applied stress.
2. Strain is completely recovered after the applied stress is removed.

To develop models for a practical design guideline, linearity was specifically defined for this investigation to satisfy only the first condition. This moves the linearity limit higher than that defined by both conditions.

To facilitate data reduction and modeling, a general equation for time-dependent creep strain may be formulated as a function of stress, time, and temperature as follows:

$$\varepsilon^c(\sigma, t, T) = Kf(\sigma)G(t)F(T) \quad (2)$$

where $f(\sigma)$, $G(t)$, and $F(T)$ are stress, time, and temperature functions, respectively. The quantity K is an environmental factor, which can be a constant or a function of stress and temperature. Since the goal of the present investigation was to develop experimentally-based models for

practical design purposes, the form of eqn. (2) was not designed to comply with the standard format of a time-temperature **shift** factor relationship. Obviously eqn. (2) must satisfy:

$$f(0)=0, \quad G(0)= 0, \quad F(T_0) = 1, \quad (3)$$

where T_0 is a reference temperature. The time-dependent deformation models were developed by obtaining proper functions and values for eqn. (2) based on experimental results obtained under various testing conditions.

From the approximate linear relationship between stress and strain observed in Fig. 1, the stress **function** $f(\sigma)$ was assumed to be a simple linear function. The time function $G(t)$ was known from experience to normally be a simple power law for creep. As the temperature dependence, an $F(T)$ function in the form of the WLF equation was considered a possible choice. Theoretically, the WLF equation is assumed to be valid in the region around T_g . It was extend here outside the intended range of applicability and the results would be verified by experimental data. Consequently, the terms in eqn. (2) were given as follows:

$$f(o) = C\sigma \quad (4)$$

$$G(t) = t^\beta \quad (5)$$

$$F(T)=\exp\left[\frac{1.8 \cdot C_1 \cdot (T - T_0)}{C_2 + 1.8 \cdot (T - T_0)}\right] \quad (6)$$

where C , β , C_1 , and C_2 are constants that were to be specified, as well as T_0 and K , based on experimental data.

To determine C , β , C_1 , C_2 , T_0 , and K for the baseline condition, the baseline temperature, $T_0 = 23^\circ\text{C}$, was specified as the reference temperature, and the environmental factor was given a value $K = 1$ for **Air/50%RH**. Then eqn. (2) can be written as follows:

$$\varepsilon^c = C\sigma \cdot t^\beta \quad , \quad (7)$$

Dividing both sides by the stress yields:

$$\varepsilon^c/\sigma = Ct^\beta \quad . \quad (8)$$

As previously pointed out, if the linear relationship between stress and strain observed in Fig. 1 is true, the data for applied stresses at 125 MPa and below should satisfy eqn. (8) and can be plotted into a single power law curve that represents the creep strain caused by a unit stress, i.e., creep compliance, as a function of time.

Figure 2 gives the experimental data in the form of creep compliance ε^c/σ vs time t . All the data in Fig. 2 fall within an error band of $\Delta\varepsilon^c/\sigma = 0.0017\%$. There is no clear trend showing the data deviations being a function of applied stress. The upper band limit is the data for 62.5 MPa instead of the highest stress of 125 MPa, while the lower limit is for 37.5 MPa instead of the lowest stress of 25 MPa. This indicates that the error band is largely a result of data scatter. The average creep deformation behavior within the linear range was thus represented by the data curve of filled squares in Fig. 2 designated as “Average of All”, which was obtained by averaging all the compliance data for given times. A least-squares fit of the “Average of All” data curve for eqn. (8) yielded:

$$C = 9.59 \times 10^{-4} \text{ and } \beta = 0.141 \quad (9)$$

The time-dependent deformation model for applied stresses within the linear range can then be obtained from eqn. (7) as:

$$\epsilon^c = 9.59 \times 10^{-4} \sigma t^{0.141} \quad (10)$$

$$\sigma \leq 125 \text{ MPa} .$$

Equation (10) is plotted in Fig. 3 with average experimental data. In many places throughout this paper, experimental data from replicated tests are averaged to smooth the scatter, and then employed to compare with the modeling results. For example, the experimental data for **25 MPa** in Fig. 3 were averaged from the results of four tests conducted at **25 MPa** under the baseline condition. Good agreement between the model and the experimental data in Fig. 3 is obvious.

It should be noted that the lab ambient air was roughly controlled only for temperature but not for humidity. Lab humidity monitor indicated that the daily relative humidity varied from approximately 30% in the winter to about 70% in the summer months. The annual average was around **50%RH**. The experimental data employed in developing eqn. (10) and presented in Fig. 3 were from the first 1,000 h of the tests conducted during the spring months when the daily relative humidity was close to **50%RH**. Many tests actually continued for about seven more months. Accelerated creep deformation was observed during the summer months, which is believed caused by seasonal humidity and probably also temperature variations because the deformation variations coincided with the local weather profile. Therefore, these should be addressed in the environmental effect section later.

Since eqn. (9) and its curve represent the elementary baseline creep deformation behavior of the material, it was used as the basis **for comparison** with the curves for other test environments.

5.2. Temperature effects in air

5.2.1. Creep compliance at various temperatures

Temperature effects on time-dependent deformation in air were investigated at -40, 50 and 120°C and compared with the baseline properties. For tests at -40°C, samples were cooled in a chamber with liquid nitrogen vapor. For tests at 50 and 120°C, the specimens were heated with a heating tape wrapped around using insulation cloth [5].

Average creep compliance curves at various temperatures were developed from the experimental data and are presented in Fig. 4. In general, the time-dependent deformation increases with temperature. However, it is noted that the curve for 50°C, although slightly higher than that for 23°C, is actually comparable to the 23°C curve since it falls into the 23°C error band, which is derived from experimental data presented in Fig. 2. It is believed that the **less-than-**expected increase in creep deformation at 50°C was caused by dehydration of the specimen. For tests at elevated temperatures, the specimens were heated throughout the testing process. Heating on one hand makes the polymeric matrix easy to deform under load, on the other hand it dehydrates the specimen. A previous investigation of the reference material indicated that dry specimens had yielded low creep deformation at room temperature [7]. Obviously, heating at 50 C was able to dehydrate the specimen but the temperature was not high enough to induce significant increase in creep deformation. Therefore, the dehydration became the dominating mechanism, which yielded deformation less than expectation.

To obtain the values of C1 and C2 in eqn. (6), test results from two extreme temperatures, -40 and 120°C, were employed to investigate the temperature-dominated mechanism in **time-**dependent deformation. To ensure the model is valid at least up to the 5,000 hour design life, the

creep strain values at 5,000 h testing time on the -40, 23 and 120°C curves were applied to eqns. (2) and (6) to yield the following values:

$$C_1 = 12 \text{ and } C_2 = 2,698 \quad (11)$$

With these values of C_1 and C_2 , the temperature function $F(T)$ in eqn. (6) is plotted in Fig. 5. The solid circles in Fig. 5 indicate the temperatures at which tests were conducted.

Creep compliance curves at various temperatures directly derived from the test data are compared with those calculated from eqn. (2) using the parameters obtained above in Fig. 6 with solid and dash lines, respectively. Note that the calculated curve for 50°C is higher than that directly derived from the test data. This indicates that the creep deformation at 50°C should be greater than the test curve if the same humidity for 23°C was maintained in the specimens at 50°C. At 120 , however, since the temperature was high enough to become the dominant effect to overpower the dehydration effect on deformation, significant creep strain yielded in spite of the dehydrated specimen condition.

5.2.2. Time-dependent deformation models for various temperatures

With the parameters obtained above, eqn. (2) can be presented as follows:

$$\epsilon^c = 9.59 \times 10^{-4} \cdot \sigma \cdot t^{0.141} \cdot \exp\left[\frac{21.6 \cdot (T - T_0)}{2698 + 1.8 \cdot (T - T_0)}\right] \quad (12)$$

where $\sigma \leq 125 \text{ MPa}$, the unit for creep strain ϵ^c is %, stress $\sigma \text{ MPa}$, and temperature $T \text{ } ^\circ\text{C}$. Creep curves for various stresses at -40, 50 and 120°C predicted using eqn. (12) are given in Figs. 7 – 9 as lines along with test data as symbols. The linear range limits for -40, 50 and 120°C were determined as 150, 100 and 75 MPa respectively as indicated by the curves in the figures.

The curves for 23°C are the same as presented in Fig. 3. Since the 50°C test data were obtained from dry specimens as discussed above, they fall consistently below the predicted curves as shown in Fig. 8. It is noted in Fig. 9 that the 120°C test data at 75 MPa hinted to rise above the predicted curve beyond 3,500 h. Analysis indicates that it is the onset of tertiary creep, which will be discussed in the next section.

5.2.3. Tertiary creep at 120°C

Although little was observed at low temperatures, tertiary creep deformation became very noticeable at 120°C, especially at low stresses. Test results indicated that at high stresses, tertiary creep was not obvious because rupture immediately followed. However, at stresses of 75 MPa and below, tertiary creep occurred without immediate rupture. Different from the tertiary creep behavior of metals, which keeps a high strain rate until rupture occurs, the tertiary creep strain rate of the present composite decelerated to the pre-tertiary level when the creep strain doubled. Figure 10 illustrates the bi-level creep strain curves at 120°C under low stresses. The inception of tertiary creep is approximately marked by arrows in Fig. 10. It appears that the lower the stress, the later the tertiary creep initiated, and the longer it might continue without rupture. Tertiary creep deformation slowed down as shown in the curves for 25 and 50 MPa. It is possible that the tertiary creep is caused by degradation mechanisms such as microcrack growth, fiber pull out etc. The high rate tertiary creep and its slowing down may signify the internal adjustment of two competing mechanisms, the damage growth and damage arrest within the composite.

For automotive structural component applications, the material is unlikely to be continuously subjected to 120°C under load for more than 100 hours since driving interruptions have to be made for refueling and resting. Therefore, tertiary creep deformation may not become a serious

design problem at 120°C. However, since it can occur at very low stresses, it should still be treated with caution in design.

Another reason for the concern of tertiary creep is that it may occur **after** very long times at lower temperatures. In an analysis using the Time-Temperature Superposition Principle (TTSP), tertiary creep was predicted to occur at 25 MPa at room temperature in the range between 9 years to several hundred years. The 9 year prediction falls within the 15 year service life and is therefore of concern. The reason for this significant range uncertainty is that the shifting operation in the TTSP analysis was performed on the log scale. Even a small amount of experimental data scatter can cause an error band of several decades in the time prediction. Unfortunately, data scatter is normally significant in random-fiber composites due to the inevitable local variation of fiber content.

5.3. Environmental effects

5.3.1. Creep compliance in various environments

Environmental effects on time-dependent deformation were investigated in distilled water at 23 and 50°C and in a simulated windshield washer fluid at 23°C. All the specimens were presoaked to ensure initial fluid' absorption before testing. Two presoak schedules were performed. The short-term presoak was conducted by immersing the specimens in the fluids at 23°C for 100 h, while the long-term presoak, only applied to distilled water, was done at 50°C for 3 months.

The creep compliance curves for the above environments are compared with that of the baseline condition in Fig. 11. It shows that creep compliance changed from low to high in the order of Air 23 C (23°C/Air/50%RH, the baseline condition), Water 23 C Short Soak (distilled water immersion at 23°C with short-term presoak), Water 50 C Long Soak (distilled water

immersion at 50°C with long-term 50°C presoak), and WWF 23 C Short Soak (windshield washer fluid immersion at 23°C with short-term presoak). Contrary to the trend, the curve for Water 23 C Long Soak (distilled water immersion at 23°C with long-term 50°C presoak) began to fall below the baseline curve after about 230 h, but remained well within the baseline error band indicated by the **arrowed** bar. Two plausible reasons for such behavior are speculated. One possibility is that the matrix was chemically or micromechanically changed during the long-term presoak at 50°C so that the polymer chains could not normally uncoil to provide time-dependent deformation. The other possibility is a gradual softening of the strain gage adhesive due to the invasive water squeezed out from the water-saturated specimen under load, resulting a low reading of strain. The latter is less likely because short-term presoak specimens may also become saturated after long-term testing. The former is better supported since similar behavior was observed in tensile tests. The average tensile strain was 2.02% in the baseline condition but it reduced to 1.52% after the long-term presoak at 50°C. For practical engineering design purposes, the long-term presoak is a condition unlikely to occur. Even if the long-term presoak could defer time-dependent deformation, it would provide no engineering advantage in the material's application because the stress-rupture property, which is known severely degraded by the long-term presoak, would limit the design life [5].

5.3.2. Time-dependent deformation models for various environments

Predictions based on the time-dependent deformation model under various stresses for distilled water immersion at 23°C after the long-term 50°C presoak were made from the creep compliance curve and are compared with the average test data in Fig. 12. A linear relationship between applied stress and creep strain was exhibited up to 50 MPa. The equation for the deformation curves valid up to 50 MPa is also presented in the figure,

The models for distilled water immersion at **23°C** after the short-term presoak, distilled water immersion at 50°C after the long-term presoak, and windshield washer fluid immersion at 23°C after a short-term presoak are compared with the corresponding average test data in Figs. 13, 14 and 15 respectively.

For practical engineering design purposes, simple environmental factors for time-dependent deformation are desirable. These factors can be developed based on the baseline condition curve. Because creep deformation varies with time, the factors should guarantee the predicting accuracy in the time range of interest. This time range was selected as 5,000 h since it is the required design operating life of an automobile in its lifetime during which the vehicle may be exposed to various service environments. The factors were derived from the ratio of the creep compliance value at 5,000 h for a specific environment to that of the baseline condition, and are presented as K_c in Table 1, where $K_c = K / F(T)$. Note that K_c includes both environmental and temperature effects. Creep compliance curves developed from test data (solid lines) are compared in Fig. 16 to those derived by multiplying the baseline curve with the environmental factors (dash lines). Obviously, the dash curves vary slightly from the solid ones at short-term but merge asymptotically into the solid curves when approaching 5,000 h.

5.4. Compressive time-dependent deformation

5.4.1. Compressive creep compliance and time-dependent deformation model in air with 50% relative humidity at **23°C**

The creep compliance curve under compression in Air/50% RH at 23°C is compared to that under tension in Fig. 17. The compressive curve represents the average behavior of only two tests conducted, and it falls within the 0.0017% error band of the tension curve. Therefore, it is assumed that the time-dependent deformation behavior of the material under tension is

comparable to that under compression, and the model for tension in **Air/50%RH** at **23°C** can be employed for compression for design purposes.

5.4.2. Compressive creep compliance and time-dependent deformation model in water at 23°C

The creep compliance data under compression at 23°C in water with the long-term presoak are compared to those under tension in Fig. 18. Obviously, the compressive data are comparable to those under tension. Therefore, the model for tension in water at 23°C can be employed for compression for design purpose, as indicated in Table 1.

5.5. Instantaneous strain under various conditions

For engineering design applications, the instantaneous deformation, i. e., the deformation that occurs upon the application of load, or so-called loading deformation, should also be considered. Experimental data of loading deformation from tests under various environments are given in Figs. 19 and 20. As stated previously, all the specimens were loaded at a constant nominal strain rate of **0.04/min.** ($6.7 \times 10^{-4}/s$). Figure 19 shows that in air most of the data points are located below the Young's modulus line, especially at high stress levels. This indicates that the instantaneous strains were slightly higher than those calculated from the Young's modulus. Figure 19 also shows that the instantaneous strains under tension at a given temperature were comparable to those under compression. Only at 120 C, the strains were slightly increased at high stresses. Figure 20 exhibits that in water and windshield washing fluid the instantaneous strains were slightly higher than the Young's modulus calculations, and compression slightly increased the strain compared to tension.

6. Summary and Discussion

For tensile loading, it has been shown that time-dependent deformation, in the linear stress-strain response range, can be approximated by a power law for room-temperature in air at 50% RH plus a series of creep-strain multiplication factors to account for other temperatures and for fluid environments. The room-temperature, ambient air creep strain is given by

$$\varepsilon^c(\%) = 9.59 \times 10^{-4} \sigma t^{0.141},$$

The temperature multipliers are given Table 1.

In a investigation of the tensile properties of the material addressed in this paper [8], two standard fluid environments are recommended for design-1,000 h presoak in room-temperature distilled water and 100 h presoak in room-temperature windshield washer fluid. The first was not one of the test conditions used for the creep tests. However creep data for test times up to several hundred hours in water at 23°C are available for a 100 h presoak. Combined, this distilled water exposure should adequately bound realistic water exposure situations. The fluid multipliers on creep strain are, consequently, distilled water 1.79 and windshield washer fluid 2.23.

Only two compressive creep conditions were examined: **Air/50%RH** at room temperature and water immersion at room-temperature after a 3-month presoak in 50°C water. In both cases, the compression results could be represented by the tensile model. On this basis, the tensile time-dependent deformation equation, together with the associated fluid factors given above, are judged to be adequate for compressive stress design use as well. However, this may not be the case for the temperature factors. It is suspected that as the temperature increases, compressive creep deformation will become larger than tensile creep deformation.

7. Acknowledgments

The author would like to thank Dr. Charles Brinkman, Dr. James Corum and Mr. Christopher Stevens for their support to this investigation; Dr. James Corum and Dr. Ken Liu for reviewing this paper. This research is sponsored by the U. S. Department of **Energy**, Assistant Secretary for Energy Efficiency and Renewable Energy, **Office** of Transportation Technologies, as part of the Advanced Automotive Materials Program.

8. References

1. Corum J., Ruggles M., Battiste R. L., Simpson W. A., McCoy H. E. and Weitsman Y. J. Durability of composites in automotive structural applications. Annual Automotive Technology Development Customers Coordination Meeting, Vol. II: Automotive R&D Poster Session. 1996. 3 13-327.
2. Karger-Kocsis J., Environmental stress corrosion behavior of polyamides and their composites with short glass fibers and glass swirl mat. Polymer Bulletin. 1991. 26: 123-130.
3. Karger-Kocsis J., and Fejes-Kozma Zs., Damage zone development and failure sequence in glass fiber mat-reinforced polypropylene under static loading conditions. Mechanics of Composite Materials. 1994. 20(1):8-13.
4. Ren W. and **Brinkman** C. R., Creep and creep rupture behavior of a continuous strand, swirl mat reinforced polymer composite in automotive environments. Proceedings of International Composites Expo '98, Nashville, TN. January 1998. Session 21-E.
5. Ren W., Investigation on stress-rupture behavior of a chopped-glass-fiber composite for automotive durability design criteria, submitted to Composite Science and Technology for publication consideration, 200 1.

6. Corum J. M. et al., Durability-based design criteria for a chopped-glass-fiber automotive structural composite. **ORNL/TM-1999/1 82**, Lockheed Martin Energy Research Corp., Oak Ridge National Laboratory. November 1999.
7. Corum J. M. et al., Durability-based design criteria for an automotive structural composite: part 2. background data and models. **ORNL-693 1**, Lockheed Martin Energy Research Corp., Oak Ridge National Laboratory. February 1998.
8. Ruggles M. B., Corum J. M., and Battiste R. L., Effects of Environment on Uniaxial and Biaxial Behavior of a Chopped Fiber Polymeric Composite, submitted to the **ASME Journal of Engineering Materials and Technology** for publication. 2000.

Table 1. Environmental creep strain multiplication factors for various conditions

Environment*	κ_c
-40°C air/T	0.59
23°C air/T&C	1.00
50°C air/T	1.24
120°C air/T	2.07
23°C water short soak/T	1.79
23°C water long soak/T&C	0.86
50°C water long soak/T	1.93
Windshield washer fluid/T	2.23

*T = tension, C = compression.

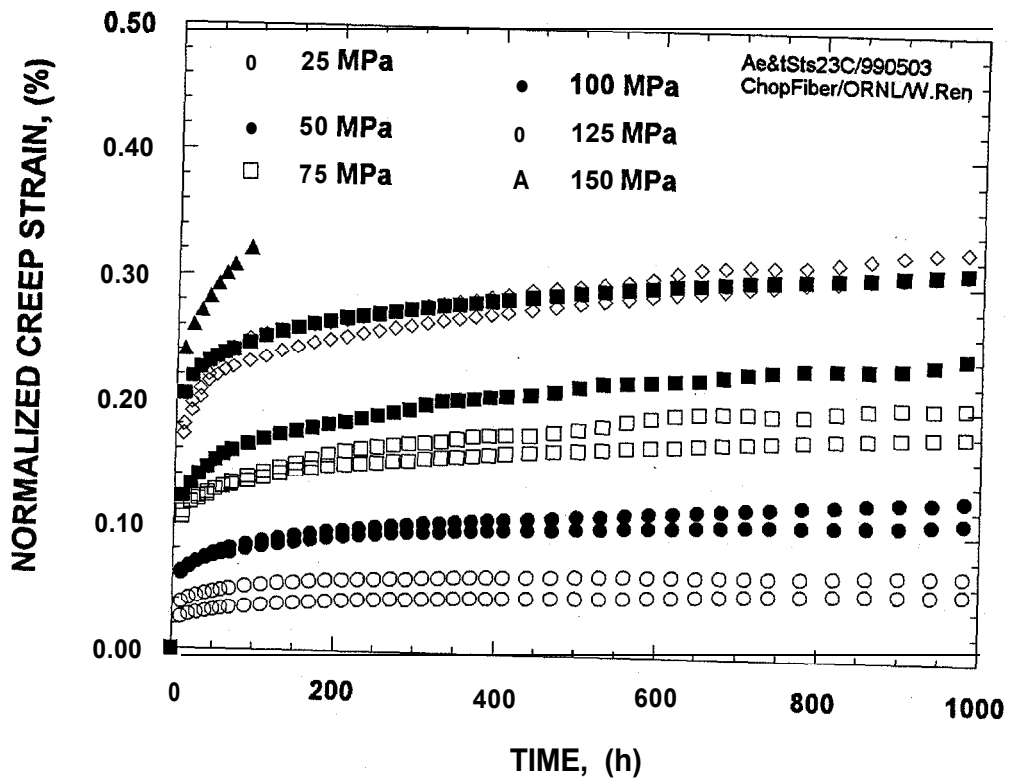


Fig. 1. Baseline experimental data indicate that **creep** strain is time-dependent and may increase proportionally to stress for tests at 125 MPa and below with some *scatters*.

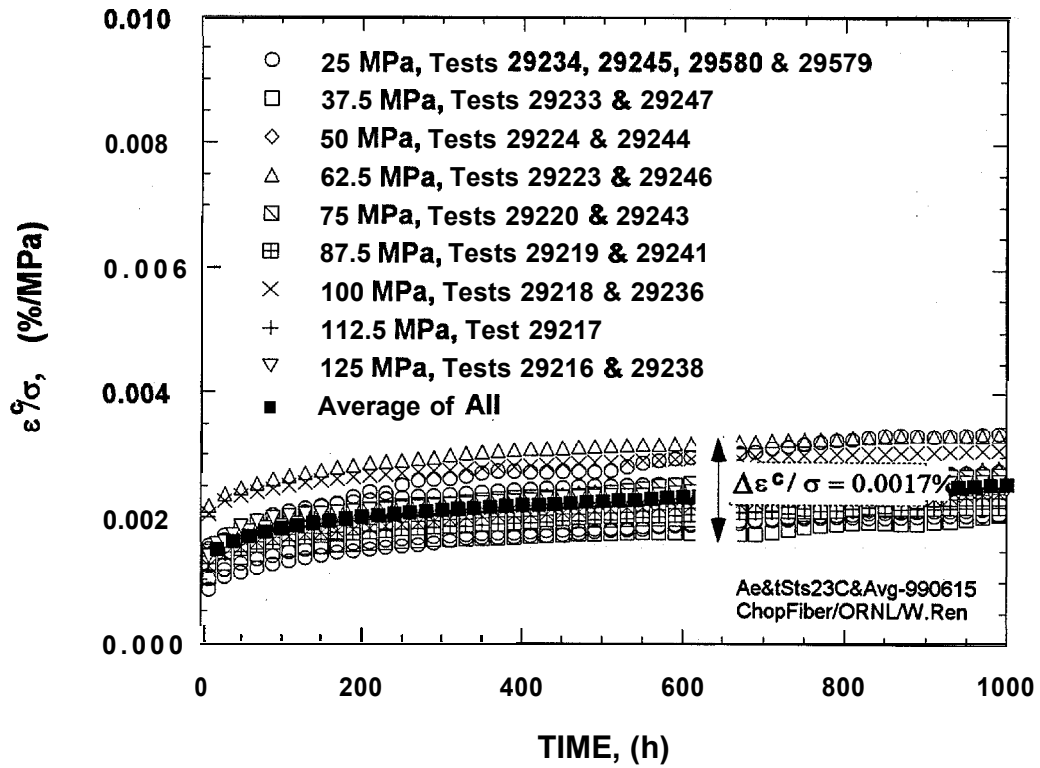


Fig. 2. Experimental data for the baseline condition in the form of time-dependent creep compliance ϵ^c/σ vs time t .

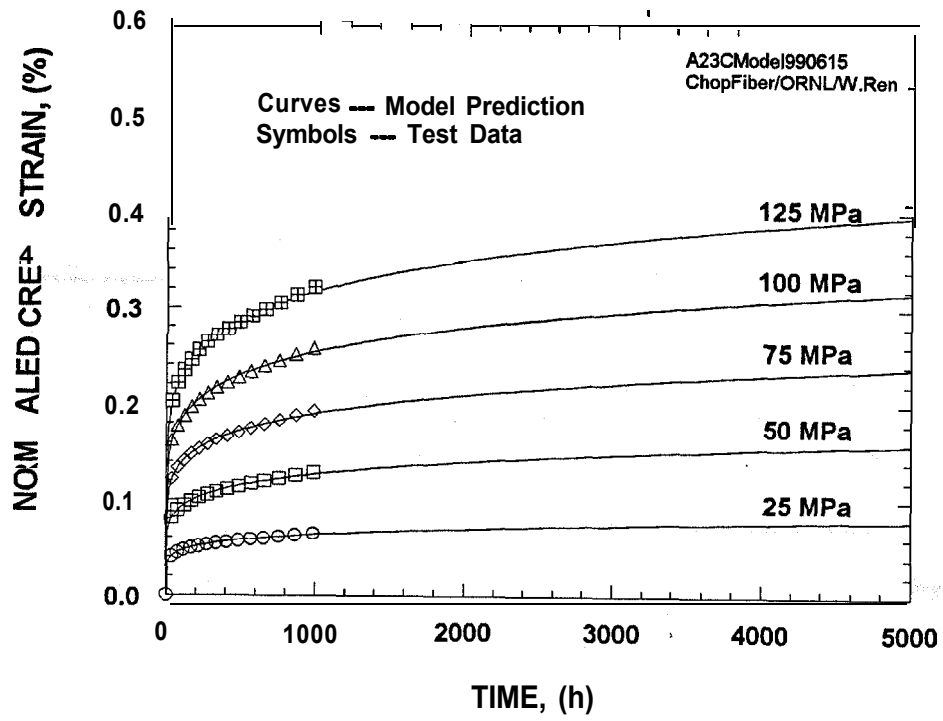


Fig. 3. Time-dependent deformation model and average experimental data for the baseline condition.

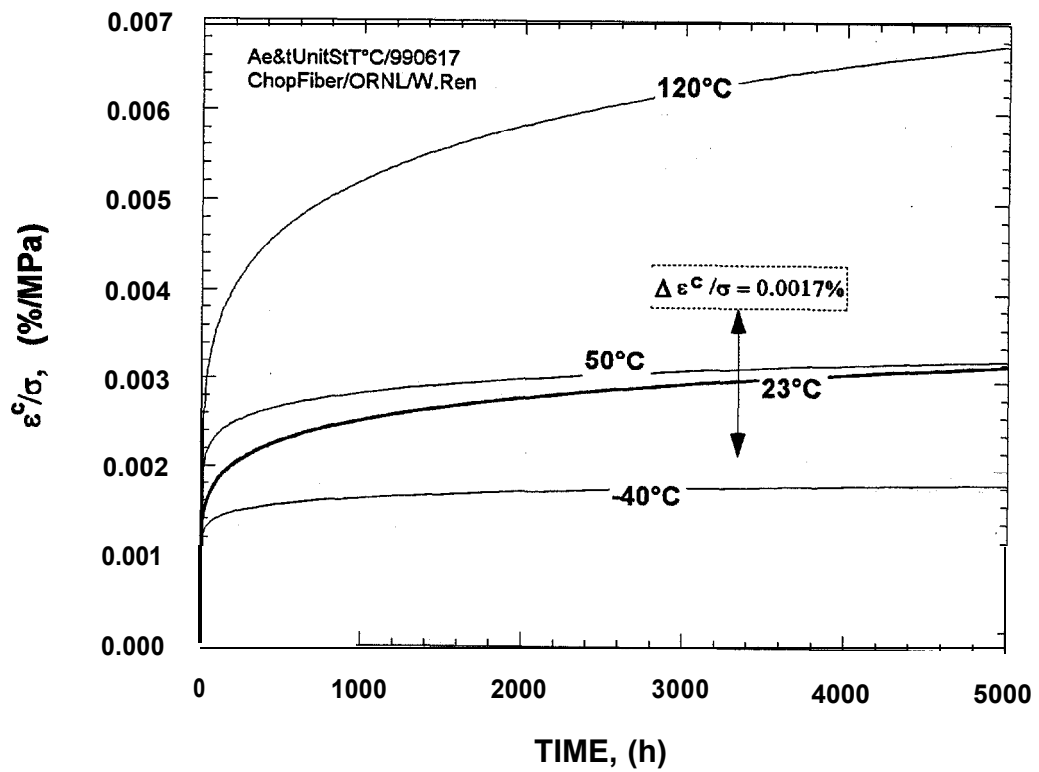


Fig. 4. Average measured creep compliance as a **function** of time at various temperatures.

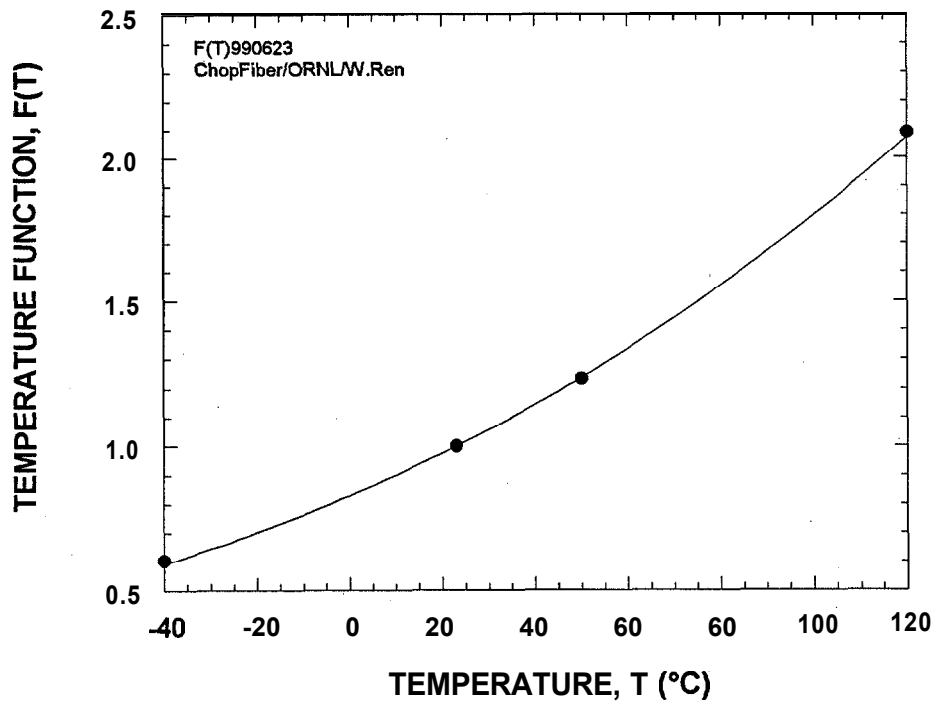


Fig. 5. Temperature function $F(T)$ employed in time-dependent deformation modeling.

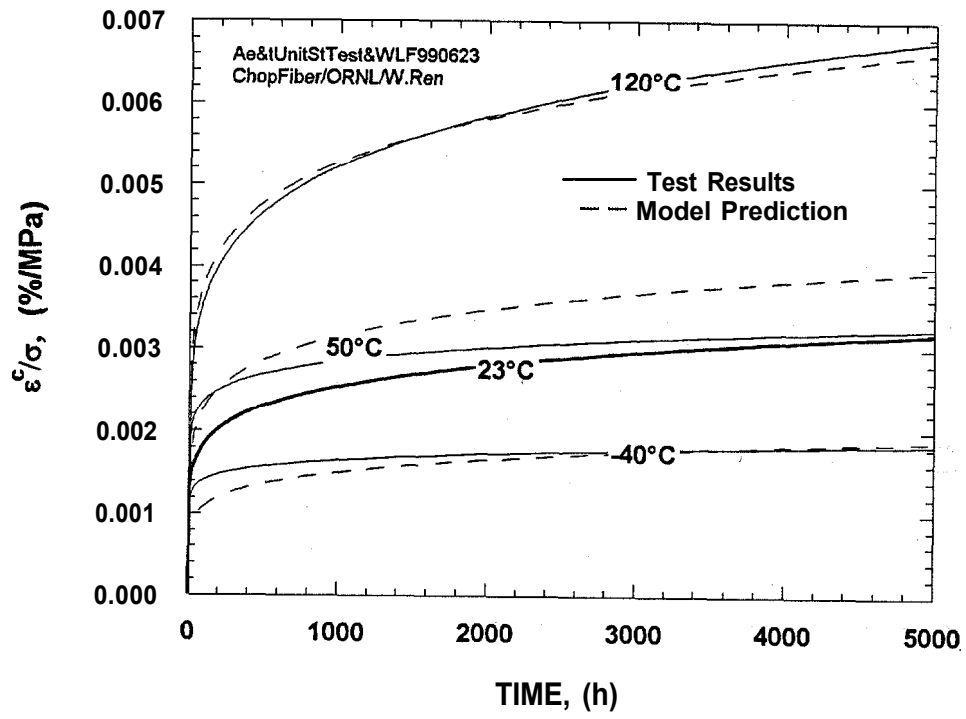


Fig. 6. Creep compliance at various temperatures directly derived from test data (solid lines) and calculated from eqn. (2) (dash lines).

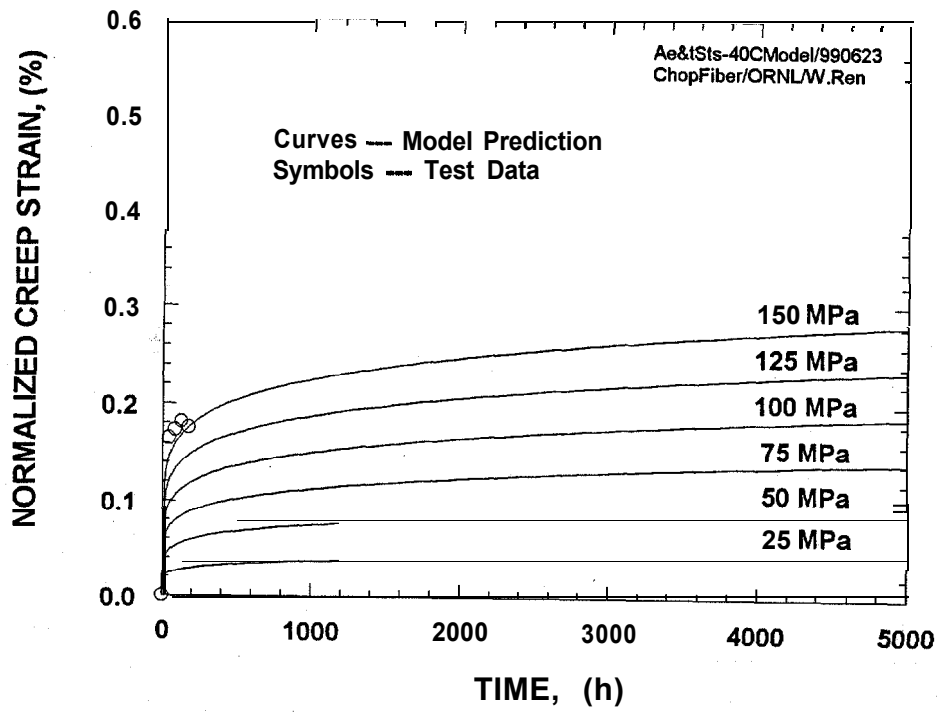


Fig. 7. Time-dependent deformation model and average experimental data for -40°C under various stresses in air.

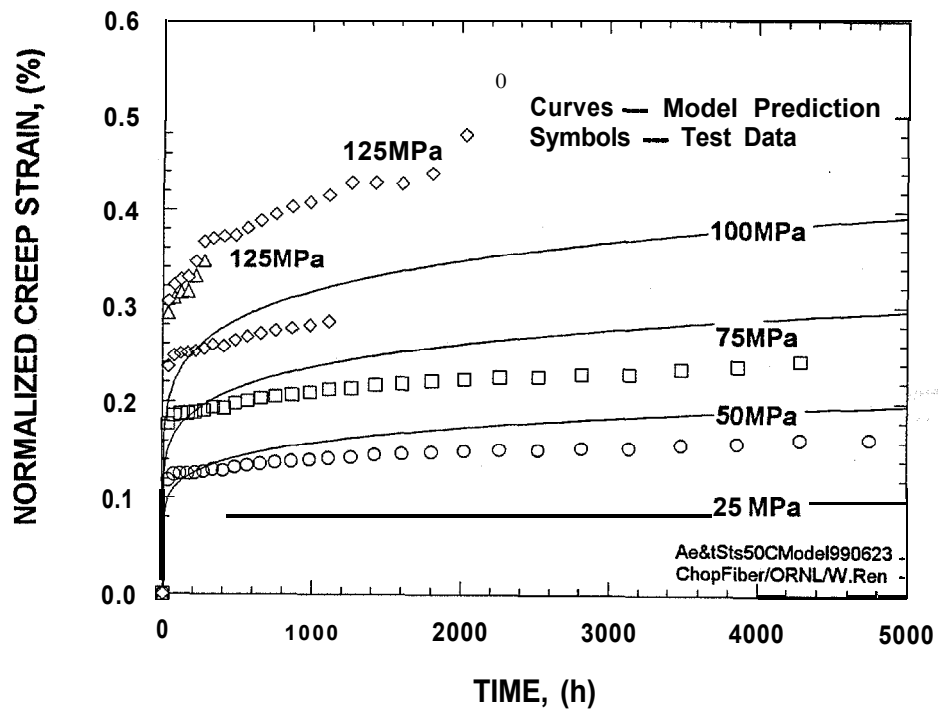


Fig. 8. Time-dependent deformation model and average experimental data for 50°C under various stresses in air.

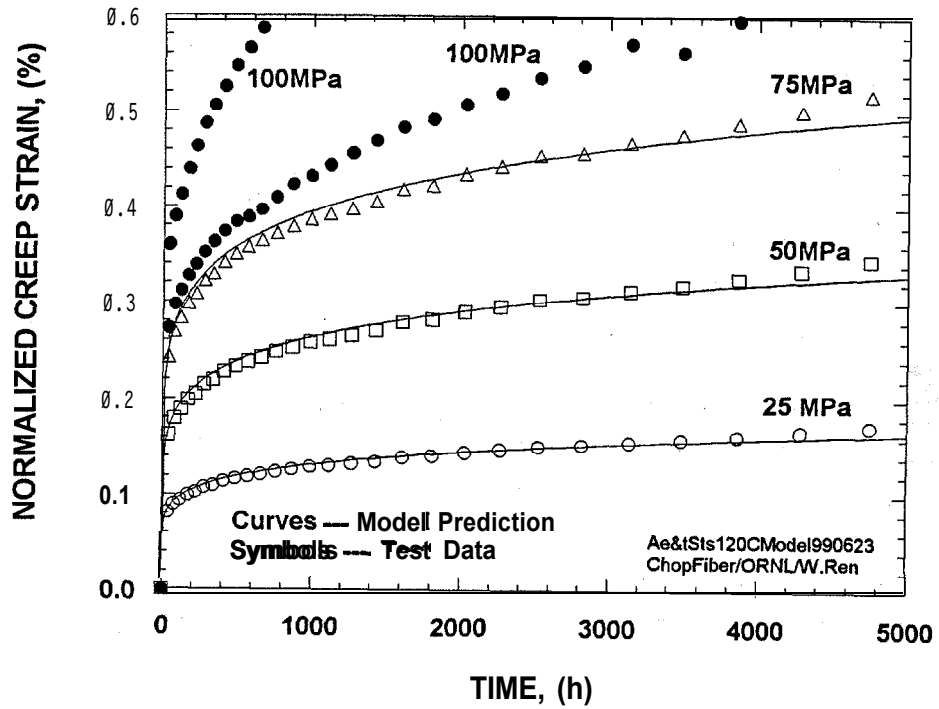


Fig. 9. Time-dependent deformation model and average experimental data for 120°C under various stresses in air.

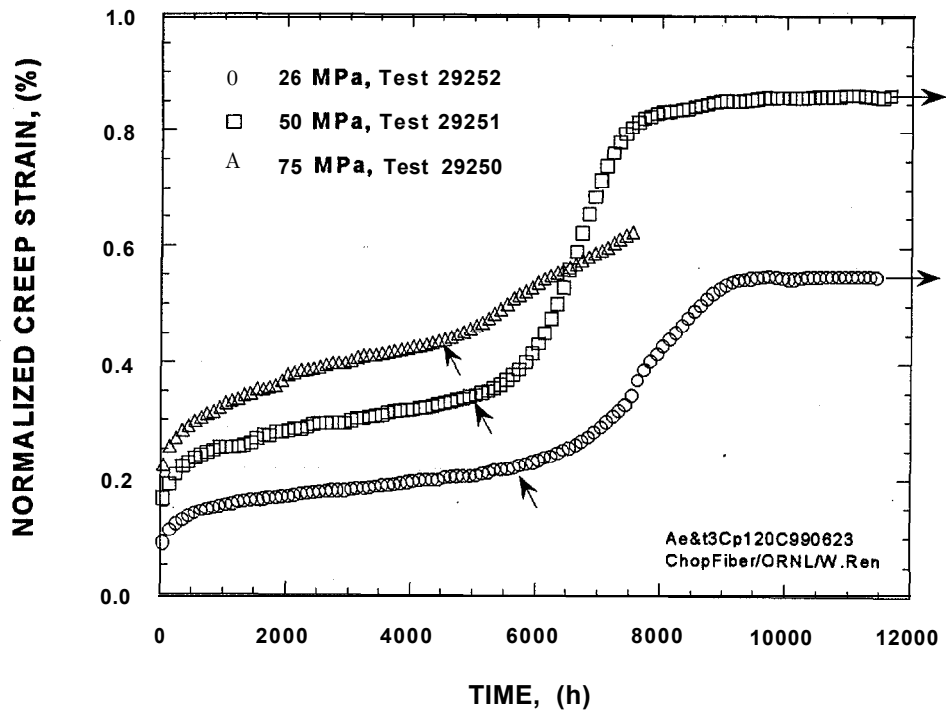


Fig. 10. Test data show tertiary creep behavior at 120°C under low stresses.

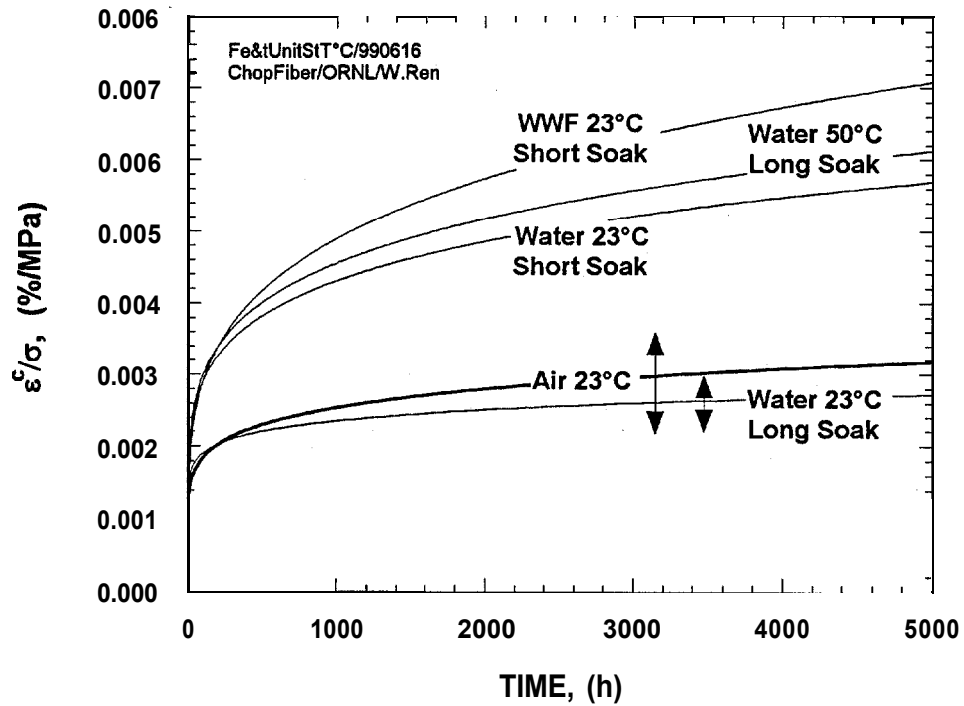


Fig. 11. Creep compliance curves for various environments. The short-term presoaks (Short Soak) in both windshield washer fluid (WWF) and water were 100 h at room temperature. The long-term presoak (Long Soak) in water was 3 months at 50°C.

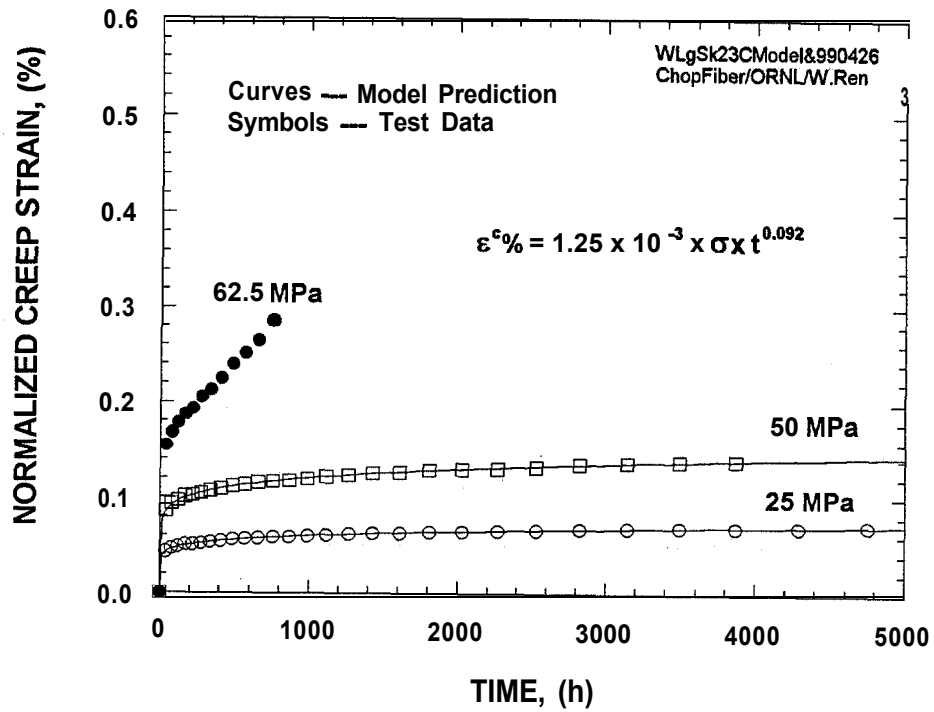


Fig. 12. Time-dependent deformation model and average experimental data for distilled water immersion at 23°C after long-term presoak at 50°C.

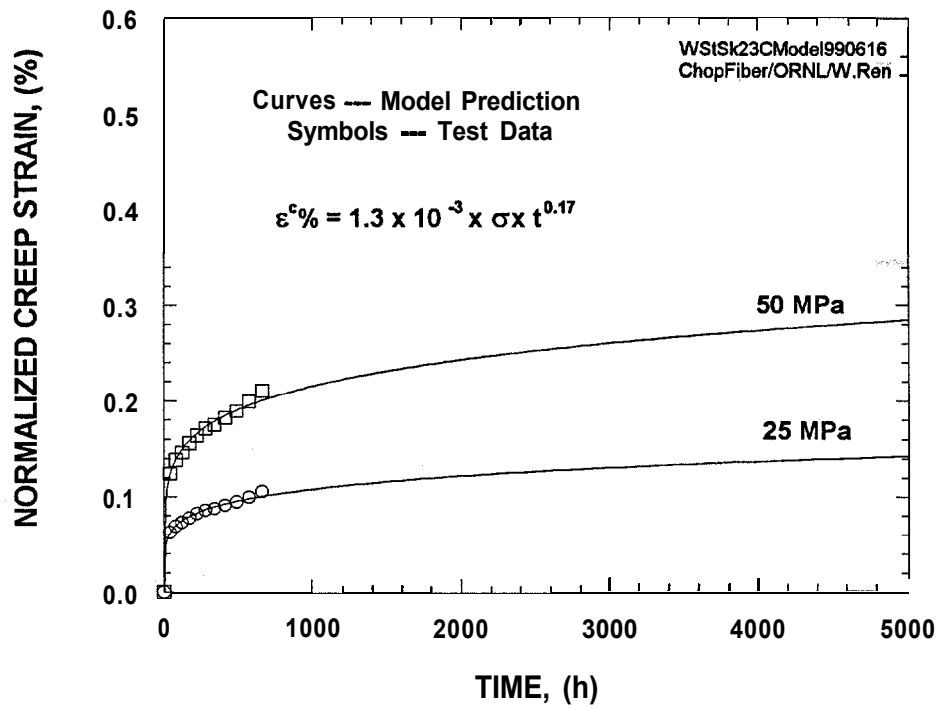


Fig. 13. Time-dependent deformation model and average experimental data for distilled water immersion at 23°C after short-term presoak at 23°C.

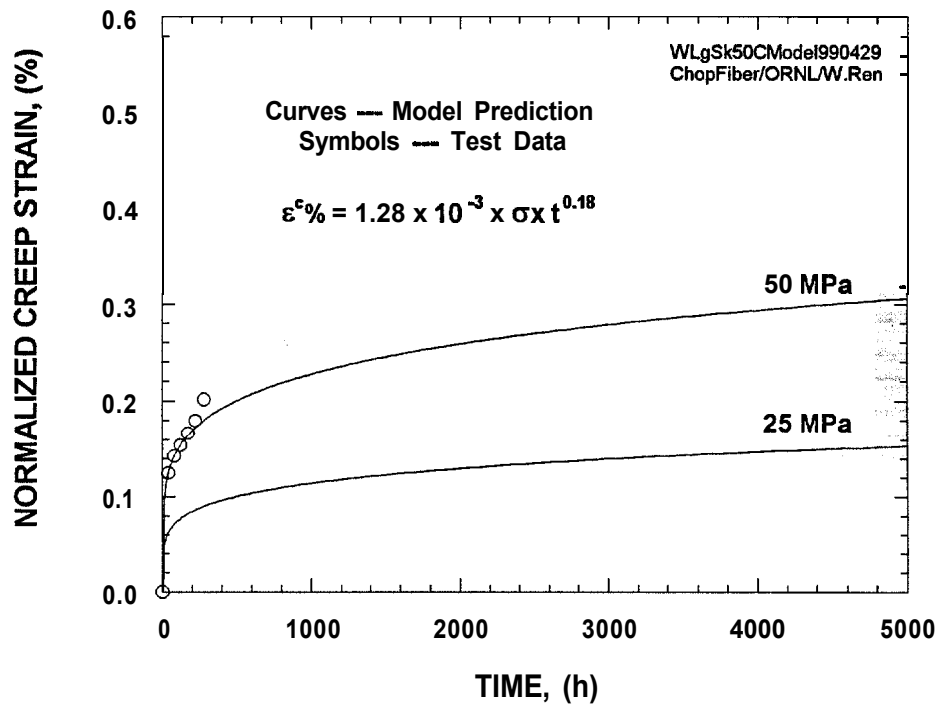


Fig. 14. Time-dependent deformation model and average experimental data for distilled water immersion at 50°C after long-term presoak at 50°C.

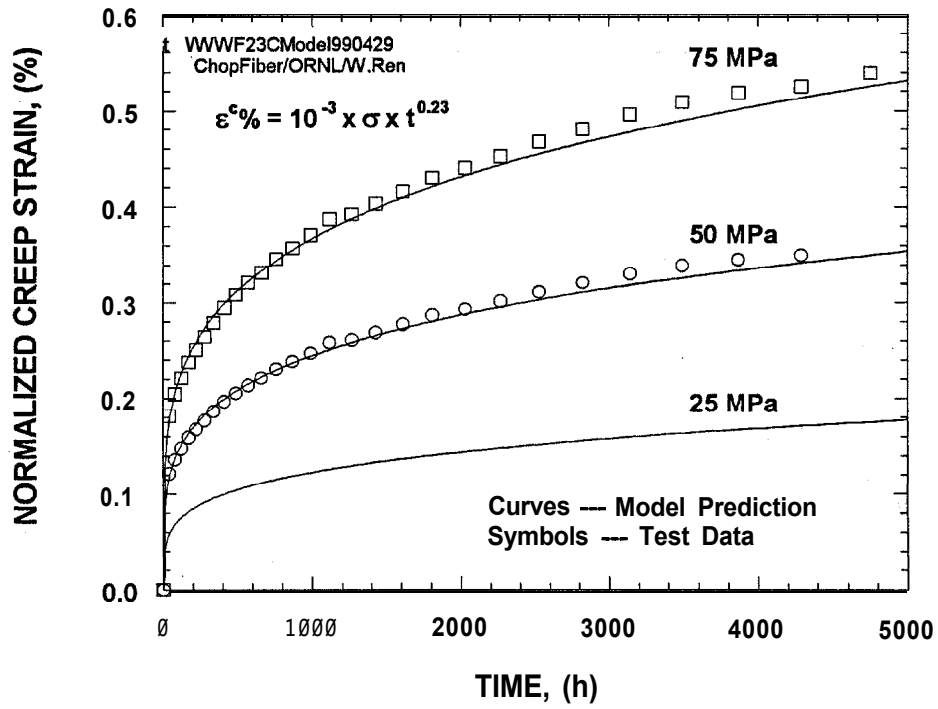


Fig. 15. Time-dependent deformation model and average experimental data for windshield washer fluid at 23°C after short-term presoak.

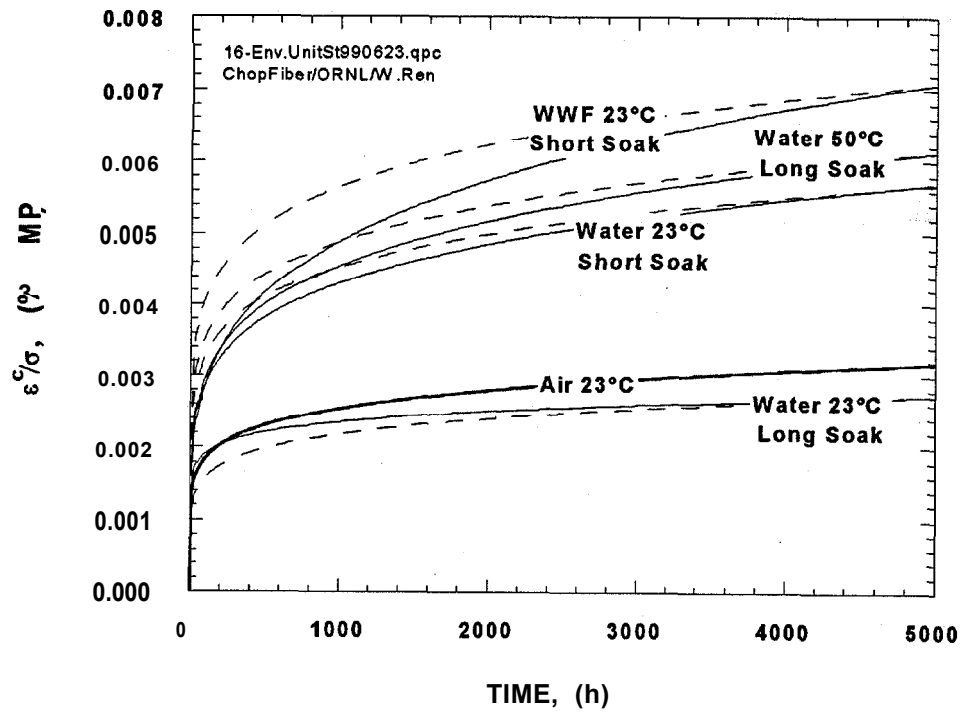


Fig. 16. Creep compliance curves developed from experimental data (solid lines), and by multiplying the baseline curve by the K_c factors (dash lines).

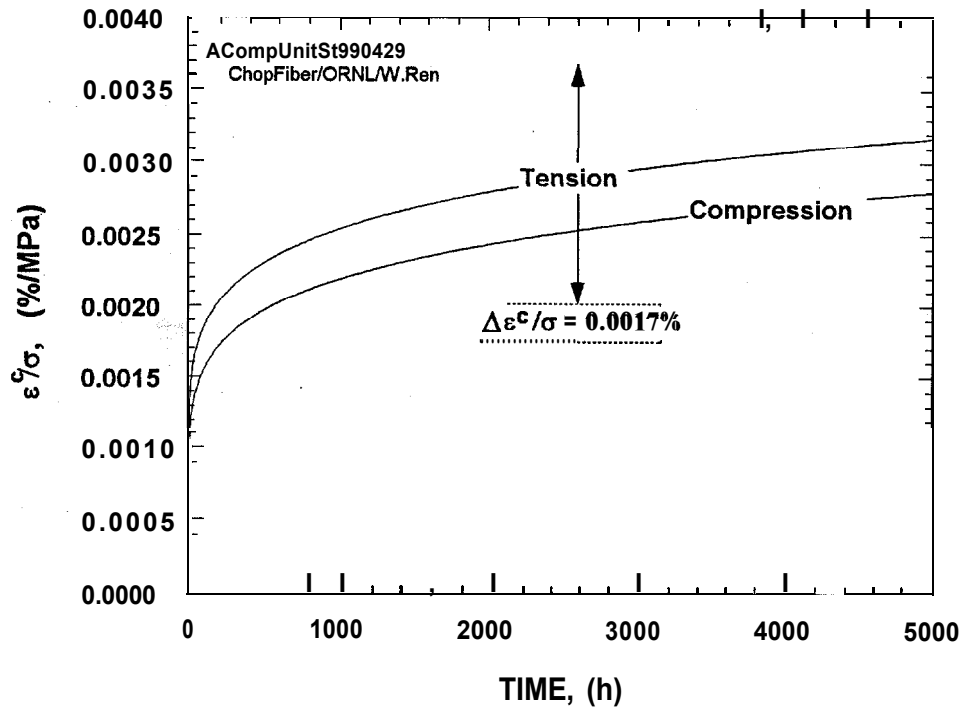


Fig. 17. Creep compliance curves under compression and tension in air with 50% RH at 23°C.

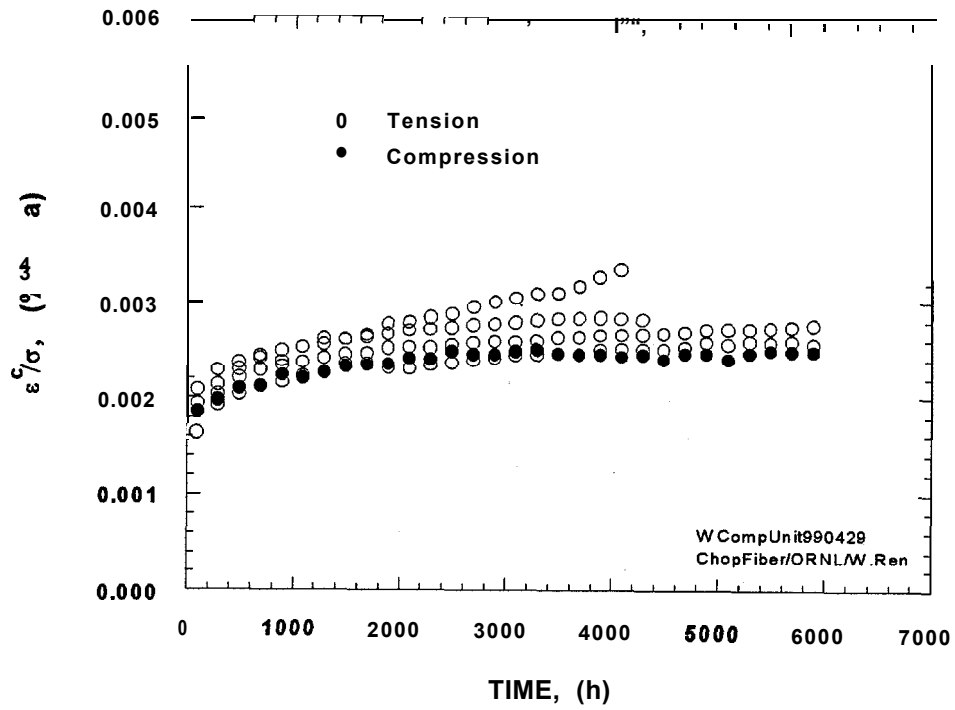


Fig. 18. Creep compliance data under compression and tension at 23°C in water with long-term presoak at 50°C.

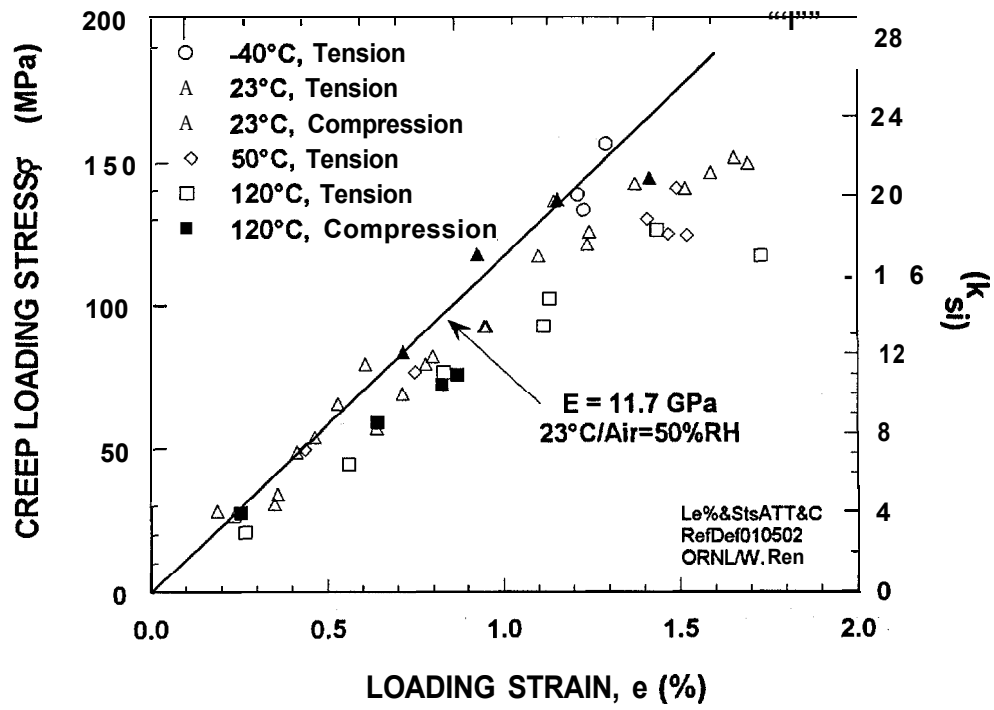


Fig. 19. Instantaneous creep strain in air at various temperatures under tension and compression.

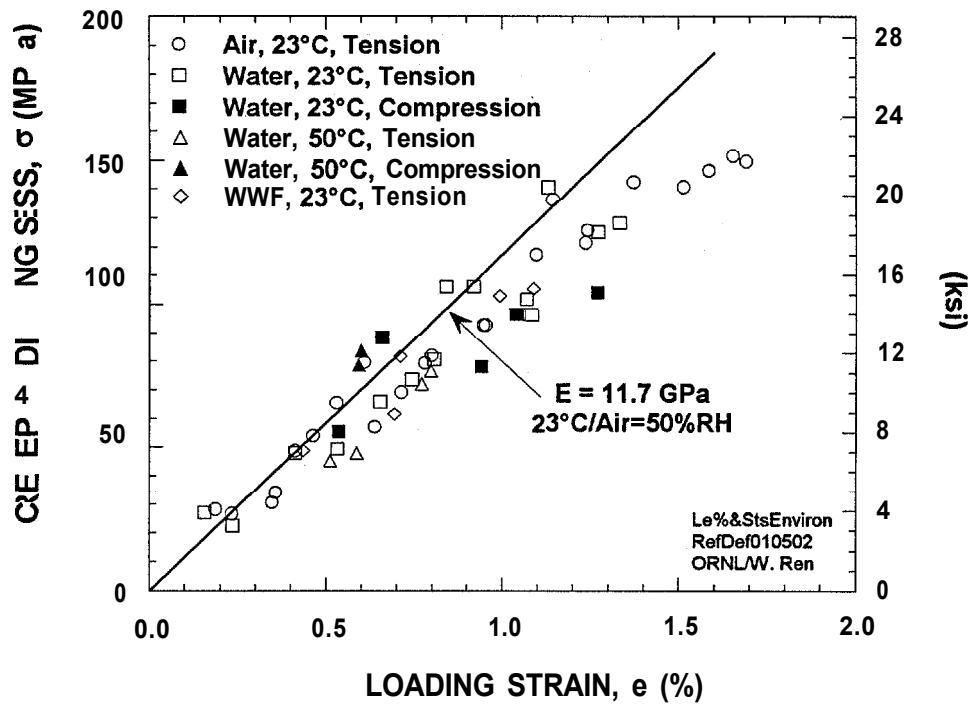


Fig. 20. Instantaneous creep strain under various fluid, temperature and load conditions.